

## Experimental Research on Structural Behaviors of Glulam I-Beam with a Special-Shaped Section

Ruyuan Yang<sup>1</sup>, Chaokun Hong<sup>2</sup>, Xiaofeng Zhang<sup>1</sup>, Quan Yuan<sup>3</sup> and Youfu Sun<sup>1,\*</sup>

<sup>1</sup>College of Materials Science and Engineering, Nanjing Forestry University, Nanjing, China

<sup>2</sup>College of Civil Engineering, Nanjing Forestry University, Nanjing, China

<sup>3</sup>College of Media and Art, Nanjing University of Information Science & Technology, Nanjing, China

\*Corresponding Author: Youfu Sun. Email: yfsun@njfu.edu.cn

Received: 05 August 2019; Accepted: 21 October 2019

**Abstract:** In order to enhance the bearing capacity of structural components, save materials, and reduce cost, a glued laminated timber (glulam) I-beam that is theoretically suitable for engineering application was proposed. In this study, 18 glulam specimens were fabricated using larch dimension lumber and resorcinol-formaldehyde resin. Four-point bending tests were carried out to compare the ultimate bearing capacity, strain, and deflection of various specimens. The results showed that: (1) The typical failure mode at bending is the web shear failure parallel to grain. Before the failure, cracks and sounds appear at the beam web, which represent the sudden brittle failure. (2) The cross-sectional strain of glulam beam changed linearly with the beam height, indicating that the plane section assumption was basically established. (3) Stiffener could improve the initial flexural stiffness of glulam beam, which experiences an increase of 28.21%. Larger the shear span ratio, smaller the initial flexural stiffness. The initial flexural stiffness improves by 10–23.5% with the increase in the thickness of the lower flange. (4) The effects of stiffener and shear-span ratio on shear strength are relatively significant. After the stiffeners are set at the support and the loading point in pairs, the shear strength of the glulam beam increases by 15.05% averagely. With the increase in the shear-span ratio, the shearing strength of the glulam I-beam gradually reduces. The equation of the shearing strength with the shear span ratio is obtained, which is shown by high fitting precision. (5) The shear strength correlation, as proposed by Soltis and Rammer, is suitable not only for rectangular beams, but also for glulam I-beams.

**Keywords:** Glulam; I-beam; stiffener; shear span ratio; flange thickness

### 1 Introduction

Timber construction refers to the engineering structure that uses timber as the major stress system. The application of timber in construction has a long history, and the most primitive architecture discovered so far was made of timber [1]. As an environment-friendly material, timber has wide range of applications due to its high strength-to-weight ratio, good thermal insulation, and relatively low price [2-4]. In recent years, extensive research efforts have been devoted to the study of bamboo and wood structures [5-12].



This work is licensed under a Creative Commons Attribution 4.0 International License, which permits unrestricted use, distribution, and reproduction in any medium, provided the original work is properly cited.

Introduction of glued laminated timber (glulam) products dates back to as early as 1800, and have been in use since the Second World War [13]. In the mid-1940s, glulam was first used in bridge engineering [14]. Owing to environmental degradation caused by excessive deforestation, the forest resources are continuously decreasing, and the development of wood structure has experienced material deficiency. Glulam overcomes various imperfections, such as knots in timber, whereas the laminates can be configured according to different stress requirements. Therefore, compared to the sawn timber having the same cross-sectional area, glulam has even moisture content, high intensity, and high permissible bending stress. Moreover, the structure of glulam is uniform, and the internal stress is small, thus it does not crack and deform easily. With good dimensional stability, the length of glulam could reach around 100 m. Nowadays, aesthetically rich and beautiful styles can be formed using glulam, which can meet the practical and artistic requirements of modern architecture. Besides, glulam with large cross-section has good flame-retardant property. The appearance of glulam has led to the rational utilization of the existing resources, and it has fully exerted the material's engineering value of "inferior material for superior use" and "large material for small use".

Many researchers have carried out a variety of studies on glulam components with different section designs and structural forms. Pulngern et al. studied the effects of section design and loading direction on the creep and fatigue properties of wood-PVC composite beam [15]. Xiong et al. [16] performed two-point loaded bending tests on 42 wooden beam specimens (12 beams with rectangular section, 24 composite T-beams, and 6 composite I-beams) to investigate the bending performance of composite beams with differently shaped sections. Chen et al. proposed a new type of bamboo-wood I-beam and studied its structural properties by investigating various parameters, including web height, shear-span ratio, and different forms of stiffeners and openings. The failure morphology and mechanism during the entire test process of these I-beams were analyzed to study the ultimate bearing capacity, ductility, and flexural rigidity and analyze the factors affecting the structural properties [17, 18]. Hassanieh et al. conducted a four-point bending test on the steel-wood composite beams and studied different modes of steel-wood composite beam using screws and bolts as shear connectors. The non-linear finite element model of steel-wood composite beam was established, and the four different failure modes of the composite beam were discussed [19]. For evaluating the flexural capacity of the glued bamboo beam, Li et al. conducted tests about the material performance and the beam flexural capacity. The strain–stress relationship was proposed based on the compressive and tensile tests parallel to strand. Furthermore, the simplified strain–stress relationship of the beam and the calculation method for ultimate bending moments and ultimate bending deformations under the three bending failure modes were proposed, which were in good agreement with the experimental results [20]. In order to enhance the utilization efficiency of timber, Shang et al. prepared hollow glulam components using larch with small diameter as the raw material and studied the flexural and lateral performances of the hollow beam-column glulam structure [21, 22]. Wang et al. [23] proposed a rectangular hollow wood column and experimentally studied its eccentric compressive properties. Tang et al. prepared and tested glulam I-beams with a span range of 2.4–7.5 m and evaluated their structural properties. They extended the length of glulam I-beams using finger joint method and connected the web and flange using two connecting modes. The failure mode, load-strain relationship, and bearing capacity of the I-beams were studied by the four-point bending tests [24]. In short, the glulam I-beams have various advantages, such as reasonable force-bearing performance, material savings, and handsome appearance. In order to expand the application range of domestic larch, a novel glulam I-beam was prepared in the current study by using domestically produced Xingan larch. The results indicate that it is of great significance to the development of wood structure in China.

In this study, the material characteristics were studied to obtain the mechanical properties of larch materials. Then, the mechanical properties of glulam I-beams were systematically investigated through

experiments. The effects of stiffeners, shear span ratios, and flange thicknesses on the structural behaviors and failure mode were studied. Moreover, the strain, deflection, and ultimate bearing capacity of various components were compared and analyzed.

## 2 Experimental

### 2.1 Materials

Larch lumbers (*Larix dahurica*) with dimension of 40 mm × 100 mm × 2000 mm were used as the raw material in this study. Their moisture contents were in the range of 9–12% after the drying treatment. Material property test was carried out on larch with reference to ASTM D143-14 [25] and the test results are presented in Tab. 1. The glulam I-beams were processed in Golden Pastrol Wood Structure Corp., Ltd., China. Referring to ANSI/AITC A190.1-2012 “Structural for Wood Products-Structural Glued Laminated timber” [26], glulam beams were processed using finger joint, assembly, and gluing. In this study, the length of finger joint was 25 mm, while the pressure of finger joint was 5.0 MPa. Resorcinol–formaldehyde resin was used for gluing, while the amount of applied glue on one side was 300 g m<sup>-2</sup>. The gluing pressure was 1 MPa, and the lamination time was 3 h. Furthermore, the curing time was 6 h.

**Table 1:** Material properties of the tested specimens

Air-dried density (g cm <sup>-3</sup> )	Tensile strength parallel to the grain (MPa)	Compression strength parallel to the grain (MPa)	Shear strength parallel to the grain (MPa)	Moisture content (%)	Number of specimens
0.61 (0.043)	71.73 (0.107)	43.64 (0.030)	8.97 (0.078)	11.86 (0.033)	20

Note: the values in bracket are coefficients of variation

Six groups of specimens were designed in this study. Each group had 3 beams, and altogether, there were 18 samples. Stiffeners, shear span ratio, and thickness of the upper and lower flanges were considered as parameters. The groups with the stiffeners in the test were Group B2–Group B6. Fig. 2 demonstrates that the stiffeners are set in pairs at the support of specimen and the web of loading point. A total of eight stiffeners were set for each specimen. The material of stiffeners was similar to that of the glulam, and had the dimensions of 25 mm × 40 mm × 120 mm. First, the adhesive surface of specimens with stiffeners was polished to be smooth finish using an abrasive paper. Then, the oil and dust impurities on the

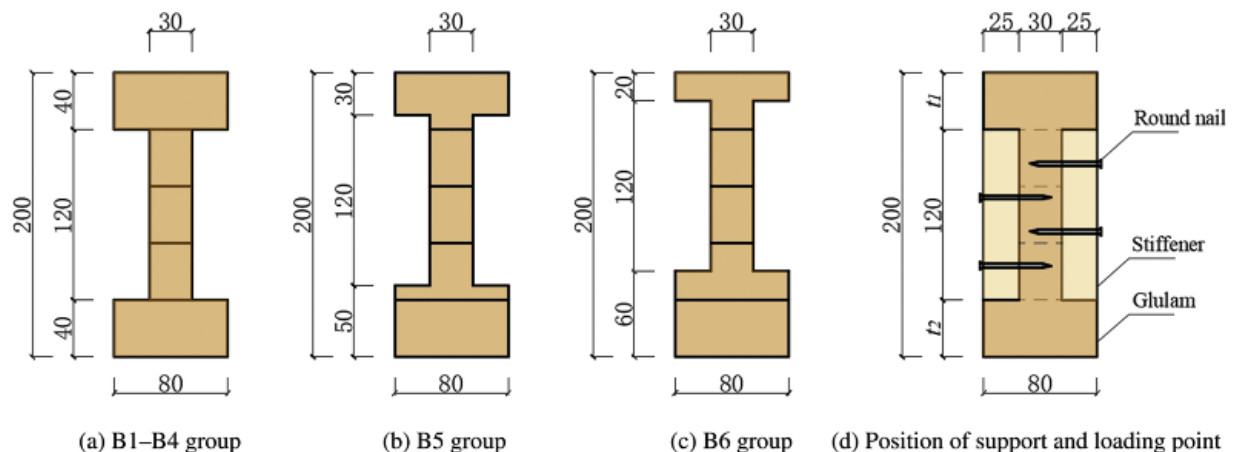


**Figure 1:** Cross-sectional configuration of specimens (mm)

adhesive surface of the component were cleaned using alcohol. Then, the stiffener was cemented using resorcinol–formaldehyde resin glue to the support and loading point of the glulam I-beam. Finally, 2.8 mm × 50 mm round steel nail was knocked in from the side of the flange at the distance of 24 mm. However, the nail space is not considered in this study. Before the adhesion between the web and stiffener reaches its designed strength, the nail only plays the role of fixation. The processed specimens were placed flat on the ground for curing for no less than 7 days.

Specific parameters of the specimens are presented in [Tab. 2](#). The overall length of the specimen was 2000 mm, whereas the margins on both ends of the support were 100 mm. This indicates that the actual span was 1800 mm. The sectional dimensions of the specimens in each group are shown in [Fig. 1](#).

**Table 2:** Parameters of the tested specimens

Specimen group	$t_1$ (mm)	$t_2$ (mm)	Reinforced	$l_1$ (mm)	$\lambda$	Number of specimen
B1	40	40	–	600	3	3
B2	40	40	Stiffeners	600	3	3
B3	40	40	Stiffeners	500	2.5	3
B4	40	40	Stiffeners	700	3.5	3
B5	30	50	Stiffeners	600	3	3
B6	20	60	Stiffeners	600	3	3

Note: where  $t_1$  is the height of upper flange,  $t_2$  is the height of lower flange,  $\lambda$  is the shear span ratio ( $\lambda = l_1/H$ ),  $l_1$  is the distance between the support and the loading place, and  $H$  is the height of beam.



**Figure 2:** Four-point bending test-site of glulam beam (mm)

## 2.2 Methods

The beams were located on the test equipment with the longer side being vertical, and the test arrangement is illustrated in [Fig. 2](#). Four-point bending test was conducted according to ASTM D198-15 [27] and GB/T 28985-2012 [28] by adopting the mode of two-point loading. The steel plates were used between the specimens and supports to prevent the contact point being damaged by over-concentrated stress. Three thimble displacement sensors (YWC-50, China) were installed on the two supports and the middle span of the beam to measure the settlement at the two supports and the deflection of the midspan. The accuracy of measurement was 0.01 mm. Strain gage 1 and strain gage 7 (model: BHF120-20AA-D150, China)

were placed at the top and bottom of the flange at the midspan, respectively. The strain gage 2 and strain gage 6 were arranged in the middle of the upper and lower flanges, respectively. Three strain gages were arranged at the web along the direction of the depth of section. Among them, one was arranged at the neutral axis of the section, while the others were arranged at equal intervals. The length direction of the strain gages was parallel to wood grain, as shown in Fig. 3. The test adopted a microcomputer-controlled electro-hydraulic servo tester. The actuator was designed with a maximum thrust of 100 kN. All measurements were acquired synchronously using the data acquisition system.

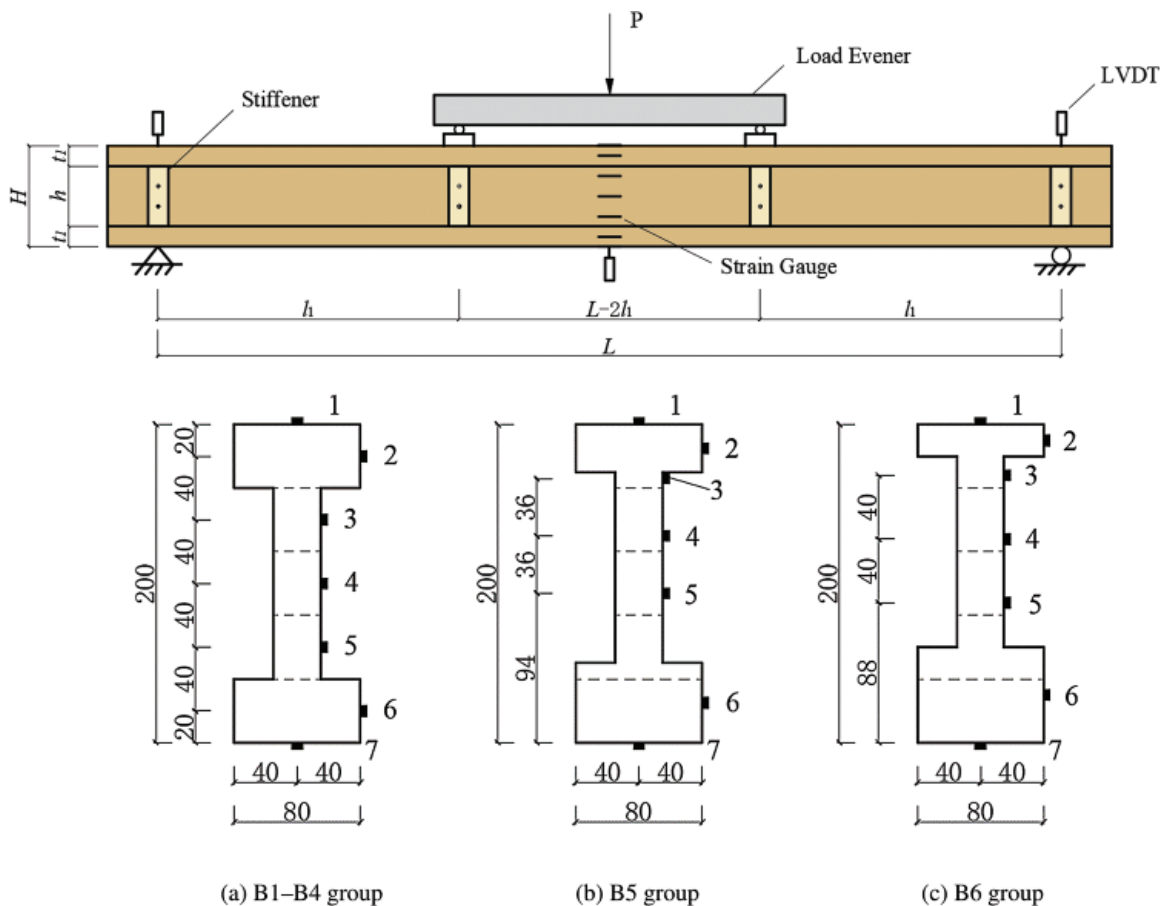


**Figure 3:** Four-point bending test point layout (mm)

Before the formal loading, it was necessary to estimate the load values,  $F_1$  and  $F_0$ . The corresponding deflection of the load increased from  $F_0$  to  $F_1$  and should be recorded. It was then unloaded to  $F_0$ . The procedure was repeated five times until the deflection did not show any obvious difference. Average value was taken for the three deflection differences as the measured deflection of the beam and the corresponding load increment is calculated by using Eq. (1) as follows:

$$\Delta F = F_1 - F_0 \tag{1}$$

where  $\Delta F$  is the load increment (kN),  $F_1$  represents the force value that is less than the proportional limit (kN), and  $F_0$  denotes the force value which is larger than the force value of the compacted specimen and device (kN).

Then, the formal loading began. The loading should be performed at a constant deformation rate. The load-displacement curve was obtained and attention was paid to the first failure, the maximum load, as well as the load and displacement of the discontinuity.

Taking B2-2 as an example, the load was applied at the rate of  $100 \text{ N s}^{-1}$  so that it increased linearly to 10 kN. Then, it was unloaded to 2 kN at the same rate. The loading process was repeated in cycle for five times to correctly calculate the elasticity modulus of the beam, after which, it was increased linearly to 20 kN at the same rate. Then, the loading method was changed into displacement control at the loading rate of  $3 \text{ mm min}^{-1}$ . The test was stopped till the test specimen was destroyed. Fig. 4 is a typical representation of the loading regime.

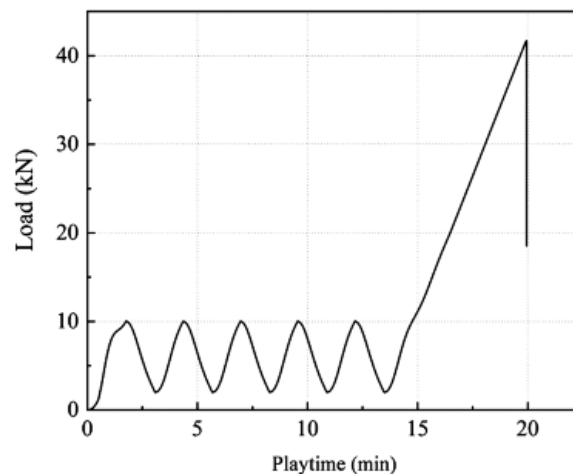


**Figure 4:** Typical loading regime (specimen B3-1)

### 3 Results and Discussion

#### 3.1 Failure Mode and Mechanism

The failure modes of glulam beams in each group were similar. At the beginning of the test, the beam was in the elastic stage, and the cyclic load was applied in this stage. After the cyclic load was completed, a small amount of plastic deformation gradually occurred as the load increased. Compared with the previous stage, the increase rate of load became slower, the deflection deformation of the glulam beam was gradually evident, and the rigidity of the beam began to decline, which indicated that the beam was in the plastic stage. When the load was in the range of  $0.75P_{\max}$ – $0.85P_{\max}$ , the beam gave out a clear cracking sound. Small cracks could be observed at the web or the bottom of the lower flange. With the continuous increase in the load, the beam produced denser sounds, while the initial cracks expanded further. The deflection deformation of the beam was significant. When the ultimate load was reached, the glulam beam got destroyed with a sudden loud noise, which belonged to brittle failure. After the unloading process, the deformed part rebounded, though some residual deformation still retained.

##### (1) Group B1 (without stiffeners)

No stiffener was set for group B1 in the test. The specimens had two failure modes, namely, the web shear deformation and cracking at the knot. The representative failure modes are shown in Fig. 5a, while the local cracks of the beam are presented in Fig. 5b. Three test specimens of this group showed serious bending and long cracks, which appeared on the web. Specimen B1-3 even exhibit penetrating cracks so that the resin at some positions is squeezed out.



**Figure 5:** Typical failure modes of group B1

(2) Groups B2–B4 (with stiffeners, but with different shear span ratios)

Transverse stiffeners were set at the supports and the loading points of groups B2–B4. The test specimens of these three groups showed three failure modes, i.e., the parallel-to-grain shear failure, cracking at the knot, and tensile failure of the wood fiber at the bottom of the flange, respectively. The shear span ratio of group B3 was small and the glulam beam showed obvious features of shear compression failure. Furthermore parallel-to-grain shear deformation occurred at the web at the loading point, which expanded to the midspan and support. The crack and the top flange formed a combined angle of  $25^\circ$ . The stiffeners were separated from the web glue line, and some of the nails were pulled out. Group B4 showed larger shear span ratio and obvious deflection deformation during the loading. The web at the lower-side of the midspan flange of specimen B4-1 was broken. The ultimate bearing capacity was far lower than that of Group 3, which indicates that the ultimate bearing capacity of specimens decreased with the increase of shear span ratio (Fig. 6).

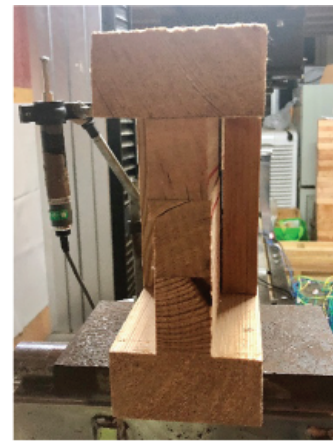
(3) Groups B5–B6 (with different upper and lower flange thicknesses)

The test specimens of groups B5 and B6 had three failure modes, which were the parallel-to-grain shear deformation, cracking at the knot, and crushing of the wood fiber at the loading point of upper flange, respectively. Most of the specimens cracked from the web at the loading point, which was the first wood shear failure and changed into glue line shear failure when the cracks extended to the support. Furthermore, obvious shear displacement was generated. Specimen B5-1 cracked at the web knot, which was the wood shear failure expanding along the grain to both ends. The upper surface of upper flange of the loading point of specimen B5-3 was crushed. The stiffener of specimen B6-2 was twisted during the loading (Fig. 7).

The compressive strength of timber parallel to the grain direction was high and the shearing strength was low in this direction, and due to the reason that the depth-span ratio of the glulam beam was large (all of which was  $1/9$  (far larger than  $1/18$ )) and the shear span ratio was small (less than 6), the bending capacity was larger than the shearing resistance. The shear strength parallel to the grain direction of timber was the weakest. Furthermore, the shear stress near the neutral axis of the beam section at the two loading points was the highest. When shear stress exceeded the ultimate shear strength, shear failure occurred, and the initial crack appeared. Owing to continuous loading, the initial crack expanded toward the midspan and was developed into a penetrating crack. This penetrating crack was the main shear crack



(a) Mode 1



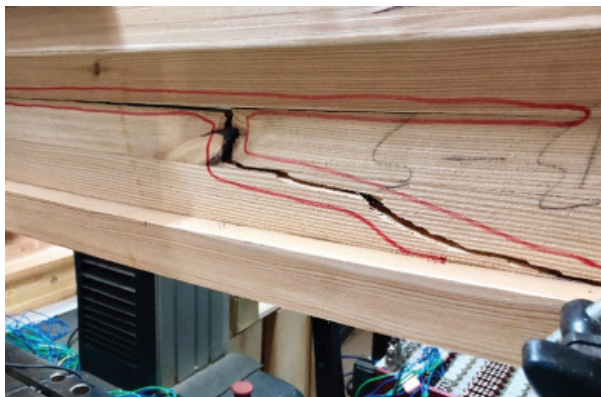
(b) Mode 2



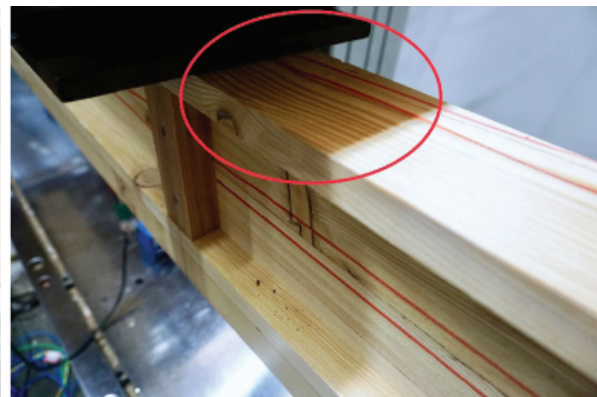
(c) Mode 3



(d) Mode 4

**Figure 6:** Typical failure modes of groups B2–B4

(a) Mode 1



(b) Mode 2

**Figure 7:** Typical failure modes of groups B5–B6

of the glulam beam. With the continuous increase in the load, the main crack expanded to the ends of beam, and the glulam beam was eventually destroyed. The main shear cracks of the glulam beams of each group were located at the downside of the neutral axis. This is attributed to the fact that when the beam is under bending load, the compression yield at the top of timber beam occurs earlier than the tension yield at the bottom, which results in gradual downward movement of the neutral axis. The position of maximum shear stress also moves down correspondingly. This indicates that the maximum shear stress occurred near the downside of the initial neutral axis of the beam section.

### 3.2 Load-Deflection Curve

The test results of all the glulam beam specimens are presented in Tab. 3. Fig. 8 shows the load-deflection curves of the test specimens of all the groups. Stiffness degradation of the beam could be classified into three stages. Stage 1 is the elastic stage, and the load-deflection curve of the specimens is approximately a straight line from the beginning of loading to the ultimate load of 75–85%. Stage 2 is from the end of Stage 1 to the ultimate load point, during which the curve presents a nonlinear

**Table 3:** Main test results

Group	$P_{\max}$ (kN)	$\omega$ (mm)	$P_n$ (kN)	$\varepsilon_c$ ( $\mu\varepsilon$ )	$\varepsilon_t$ ( $\mu\varepsilon$ )	$\tau$ (MPa)	$K$ (N mm <sup>-1</sup> )
B1-1	37.97	23.92	10.61	-6700	5897	4.25	1.52
B1-2	40.94	38.00	9.80	-5338	4910	4.59	1.44
B1-3	39.82	22.61	12.38	-5662	5090	4.40	1.73
Mean	39.577	28.177	10.930	-	-	4.413	1.563
SDV	1.225	6.967	1.077	-	-	0.139	0.122
COV	0.031	0.247	0.099	-	-	0.032	0.078
B2-1	46.23	22.53	13.68	-6610	6562	5.18	1.97
B2-2	46.34	20.24	14.94	-6030	5890	5.19	2.14
B2-3	42.21	19.99	12.71	-6320	6310	4.73	1.90
Mean	44.927	20.920	13.777	-	-	5.033	2.003
SDV	1.921	1.143	0.913	-	-	0.215	0.101
COV	0.043	0.055	0.066	-	-	0.043	0.050
B3-1	66.52	29.39	16.48	-5700	5540	7.45	2.40
B3-2	57.07	23.26	16.43	-6170	5760	6.39	2.32
B3-3	44.18	17.18	18.17	-5530	5020	4.95	2.52
Mean	55.923	23.277	17.027	-	-	6.263	2.413
SDV	9.156	4.985	0.809	-	-	1.025	0.082
COV	0.164	0.214	0.047	-	-	0.164	0.034
B4-1	24.30	11.77	15.93	-6180	5802	2.72	2.09
B4-2	25.54	12.12	14.85	-5996	5902	2.86	1.98
B4-3	23.84	36.60	12.45	-6124	6002	2.67	1.78
Mean	24.560	20.163	14.410	-	-	2.750	1.950

(Continued)

**Table 3 (continued).**

Group	$P_{\max}$ (kN)	$\omega$ (mm)	$P_n$ (kN)	$\varepsilon_c$ ( $\mu\varepsilon$ )	$\varepsilon_t$ ( $\mu\varepsilon$ )	$\tau$ (MPa)	$K$ (N mm <sup>-1</sup> )
SDV	0.718	11.623	1.454	–	–	0.080	0.128
COV	0.029	0.576	0.101	–	–	0.029	0.066
B5-1	51.85	23.22	15.26	–6280	6404	5.84	2.24
B5-2	56.14	26.18	14.87	–6300	6387	6.32	2.11
B5-3	32.40	17.38	16.05	–6560	6691	3.65	2.24
Mean	46.797	22.260	15.393	–	–	5.270	2.197
SDV	10.330	3.656	0.491	–	–	1.162	0.061
COV	0.221	0.164	0.032	–	–	0.221	0.028
B6-1	49.44	20.97	17.31	–4500	3226	5.65	2.36
B6-2	51.64	21.10	17.71	–4286	3152	5.90	2.26
B6-3	42.97	15.66	20.36	–4714	3300	4.91	2.79
Mean	48.017	19.243	18.460	–	–	5.487	2.470
SDV	3.680	2.534	1.353	–	–	0.420	0.230
COV	0.077	0.132	0.073	–	–	0.077	0.093

Note: where  $P_{\max}$  is the ultimate load of specimens,  $P_n$  is the ultimate load of specimens under normal service condition (load when midspan deflection is  $l/250$  of the span of beam),  $\omega$  is the midspan deflection under ultimate load,  $\tau$  is the shear strength of specimens,  $K$  is the initial flexural stiffness of specimens (secant stiffness for  $0.1P_{\max}$ – $0.4P_{\max}$  of each specimen), and COV denotes coefficient of variation, SDV represents the standard deviation.

characteristic. In this stage of stiffness degradation, the beam gradually produces cracks parallel to the grain, which continue to expand with the increase of load. Stage 3 is the failure stage. For most of the test specimens, when the ultimate load was reached, the shear failure parallel to the grain of glulam beam occurred, and the load decreased rapidly. Only group B3 with a larger shear span ratio had shear failure along the grain. After this, bending failure occurred, and the wood fiber at the bottom of the midspan section flange got destroyed. The failed specimens of each group showed no ductility and the failure happened suddenly. When the midspan deflection is less than the serviceability limit (the midspan deflection is less than  $l/250$ , which is equal to 7.2 mm in the current study), the load-deflection curve is basically a straight line, which is consistent with the experimental phenomenon that the test specimens have no obvious damage during this stage.

Figure 8 demonstrates that the stiffener can effectively improve the ultimate bearing capacity of glulam I-beam, which has an average increase of around 14.04%. Furthermore, the shear span ratio significantly affects the ultimate bearing capacity of specimens. For the larger shear span ratio, the ultimate bearing capacity is lower. For the same cross-sectional areas, if the thickness of bottom flange increases, the bearing capacity of the timber beam also increases by 11.70–33.96% in normal service. It is stipulated in GB/T50005 2017 that, under the serviceability limit state, the deflection of beam should be less than  $l/250$  (where  $l$  is the calculated span of beam) [29]. In this study, the average deflection of the glulam beam to the ultimate load is 22.34 mm, which is far higher than the maximum allowable design value of 7.2 mm. It is about 3.1 times the design value. Therefore, the key design index of the glued I-beam is usually the deflection deformation instead of the strength. The reason to select deflection instead of strength is that, it can be measured directly through a beam test. The strengths of all the glulam beams in the tests have residuals to some degrees.

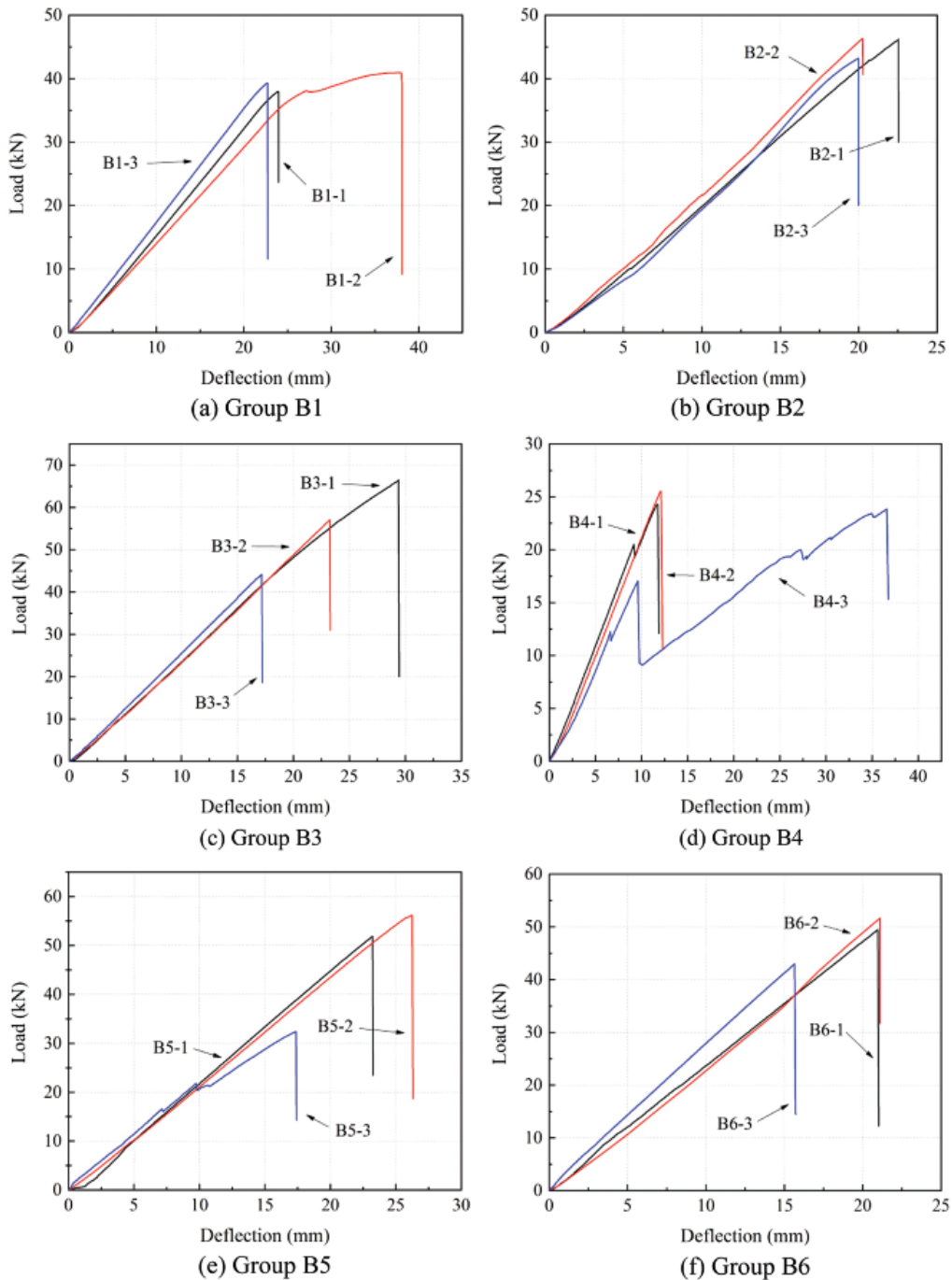


**Figure 8:** Load-deflection curves

### 3.3 Section Strain Distribution

With the increase in the load, the deflection of glulam beam gradually increased, and the strain on the beam section gradually increased. Fig. 8 shows the distribution of strain on the midspan section of the glulam of all groups along the section height  $h$ . Fig. 9 shows that  $P_{max}$  is the ultimate load and one specimen was selected from the three specimens of each group to perform analysis. Clearly, during the loading process, as

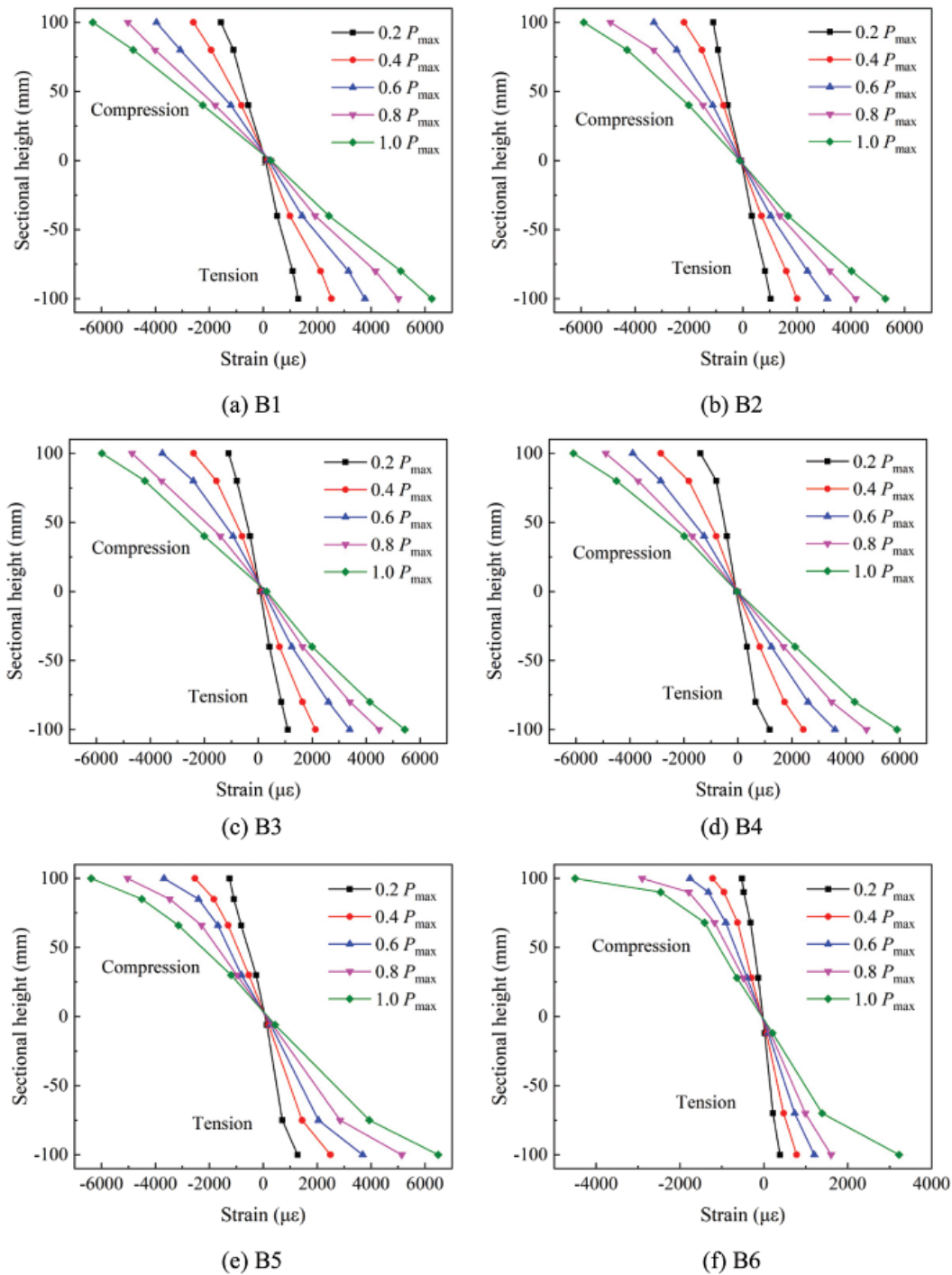


**Figure 9:** Development of the strain profile for the mid-span cross-section

the load increases, the strain on the midspan section maintains a linear relationship, indicating that the plane section assumption is established, and the influence of the shear stress can be ignored. The envelope line is approximately linear from the start of loading to the failure of test specimen, which indicates that the strain at each point of the cross-section is directly proportional to the neutral axis distance. When the specimen

approaches failure, the average maximum tensile strain and the compressive strain of wood fibers in each group are 5436 and 5833  $\mu\epsilon$ , respectively. These values show that the tension performance of the timber is different from the compression performance and verify the conclusion that, during the bending process of the beam, the wood fiber in the top compressive area of the section yields earlier.

Figures 10a and 10b show the load-strain curves of the upper and lower surfaces of the midspan of glulam beam B2-3 and B6-1. In the initial stage, the elastic moduli in the tension area and the compression area of the beam are basically consistent with each other. However, the compressive strain of the top surface deviates from the initial tangent modulus line earlier than the bottom tensile strain. This is attributed to the fact that the tensile strength of the wood is greater than the compressive strength, thus the compression area enters plasticity earlier than the tensile area.

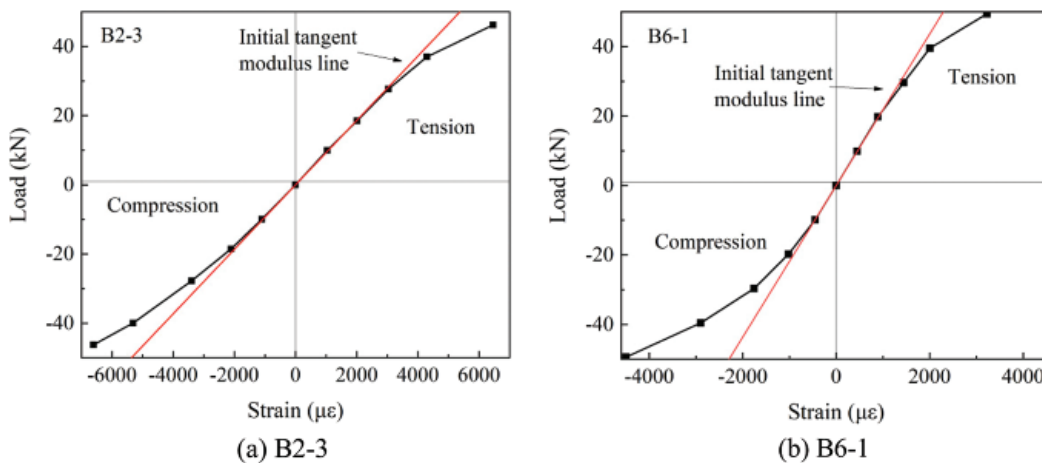


Figure 10: Typical load-strain curves for the mid-span cross-section

Figure 11 shows the load-neutral axis height curve of a typical specimen. During the loading process, the neutral axis offsets from the initial position to the tension side of the beam’s bottom, in particular, in the later stage of loading process. As the load reaches the elastic limit, the wood fiber in the compressed zone gradually enters the plasticity stage; the decreasing compression elastic modulus results in the re-distribution of internal stress inside the section, thus the neutral axis moves downward and reaches a new balance state.

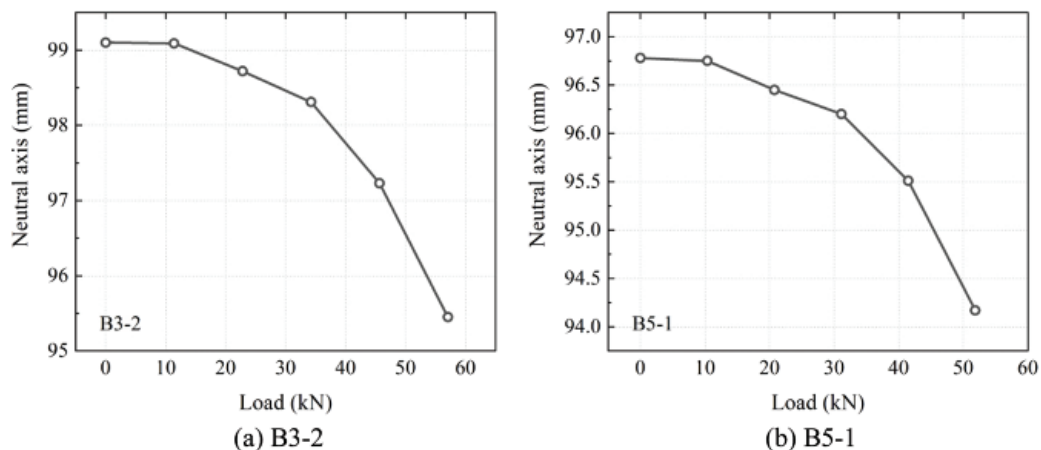


Figure 11: Descent of neutral axis during loading process

### 3.4 Analysis of Factors Affecting the Initial Flexural Stiffness of Glulam Beams

According to the design calculation method of Japanese timber structure [30, 31], the two points with the load values of  $0.1P_{\max}$  and  $0.4P_{\max}$  were connected in a straight line, and the slope of this straight line was taken as the initial flexural stiffness ( $K$ ) of the specimen. The test results were analyzed via variance analysis and the analysis results are presented in Tab. 4. At the level of  $\alpha = 0.05$ , the significance of the effects of stiffener, shear-span ratio, and flange thickness on the initial flexural stiffness are 0.02, 0.01, and 0.05, respectively, indicating that the effects of stiffener and shear-span ratio on initial bending stiffness are more obvious and the flange thickness has a certain and not significant effect.

**Table 4:** Variance analysis on the initial flexural stiffness under different factors

Factors	Source	SS	DF	MS	F value	Significance
Stiffeners	Inter-group	0.29	1	0.29	15.42	0.02
	Intra-group	0.08	4	0.02	–	–
	Total	0.37	5	–	–	–
Shear span ratio	Inter-group	0.39	2	0.19	11.55	0.01
	Intra-group	0.10	6	0.02	–	–
	Total	0.49	8	–	–	–
Thickness of flange	Inter-group	0.33	2	0.16	4.94	0.05
	Intra-group	0.20	6	0.03	–	–
	Total	0.53	8	–	–	–

Note: where SS indicates sum of squares, DF denotes degree of freedom, and MS represents mean squares.

The comparison between average initial flexural stiffness of each specimen group is shown in Fig. 12. Stiffeners could improve the initial flexural stiffness of glulam beams. The initial flexural stiffness of specimens of group B2 improves by around 28.21% compared to that of group B1. For a higher shear span ratio (groups B2, B3, and B4), the initial flexural stiffness is smaller. The initial flexural stiffness could improve by around 10–23.5% if the thickness of lower flange is increased (groups B2, B5, and B6).

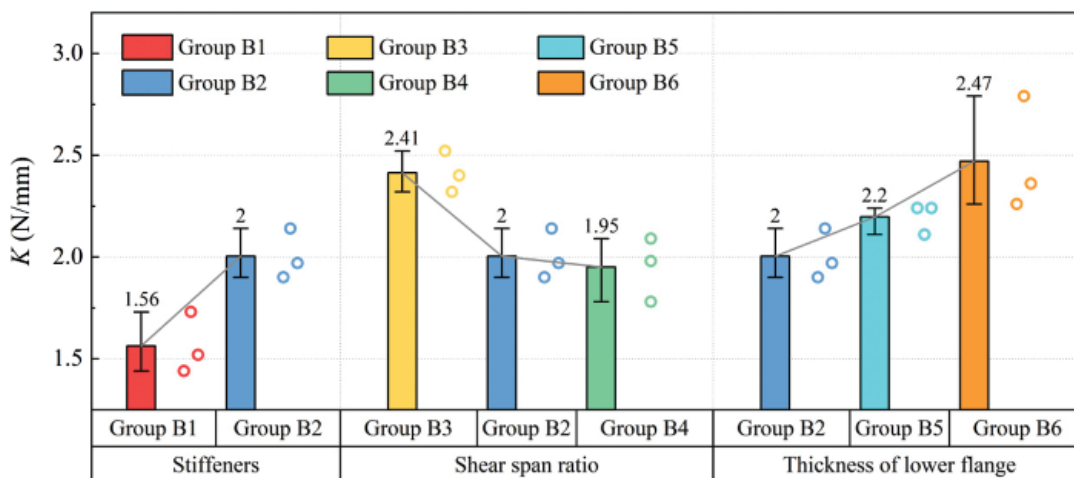


**Figure 12:** Comparison of initial flexural stiffness

### 3.5 Analysis of Factors Affecting the Shear Strength of Glulam Beams

Table 5 presents the results of the variance analysis carried out on test results. At the level of  $\alpha = 0.05$ , the significance of the presence or absence of stiffeners on shear strength is 0.03, indicating that the stiffener has a certain effect on the shear strength. The significance of the shear-span ratio on the shear strength is 0.00, indicating a significant effect on the shear strength. The significance of flange thickness on the shear strength is 0.83, indicating a slight effect on shear strength. This may be attributed to the fact that the span-depth ratio of specimen is relatively small so the shearing effect has a more significant effect on the deformation of the member. It was thus recommended to increase the span-depth ratio in the subsequent tests to investigate the effect of flange thickness on the bearing performance of the glulam I-beam under the flexural moment.

**Table 5:** Variance analysis on the shear strength under different factors

Factors	Source	SS	DF	MS	F value	Significance
Stiffeners	Inter-group	0.58	1	0.58	11.76	0.03
	Intra-group	0.20	4	0.05	–	–
	Total	0.77	5	–	–	–
Shear span ratio	Inter-group	19.07	2	9.34	17.30	0.00
	Intra-group	3.31	6	0.55	–	–
	Total	22.38	8	–	–	–
Thickness of flange	Inter-group	0.31	2	0.15	0.20	0.83
	Intra-group	4.72	6	0.79	–	–
	Total	5.03	8	–	–	–

Note: where SS denotes sum of squares, DF represents degree of freedom, and MS denotes mean squares.

When the stiffeners are set at the support and loading point in pairs the shear strength of glulam beam increases by 15.05% averagely, as shown in Fig. 13. Fig. 14 shows the relationship between the shear strength and shear span ratio of glulam beam. Fig. 11 demonstrates that the shear strength of glulam beam gradually decreases with the increase in shear span ratio. The decrease is almost linear with the increase in shear span ratio. Regression analysis of the experimental data yields an equation between the

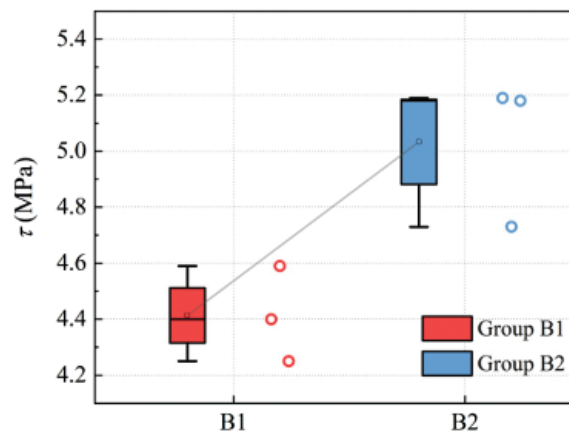


**Figure 13:** Effect of stiffener on shear strength

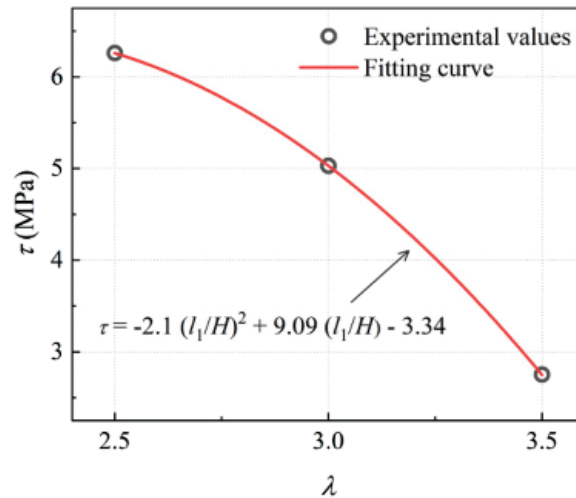


**Figure 14:** Relationship between shear strength and shear span ratio

shear strength and shear span ratio, whose coefficient of determination ( $R^2$ ) is 1 and shows a high precision of fitting (see Eq. (2)).

$$\tau = -2.1(l_1/H)^2 + 9.09(l_1/H) - 3.34 \quad (2)$$

where  $l_1$  is the length from the support to the loading point (mm) and  $H$  is the depth of the beam (mm).

### 3.6 Calculation of the Shearing Strength

The glulam beam is a type of laminar composite material; therefore, the normal stress on laminar and the interlaminar shear stress are responsible for the failure. The shear span ratios of glulam beams of each group vary within 2.5–3.5, all of which are less than 6. The shear span ratio is relatively small; therefore, the interlaminar shear stress is a factor that cannot be ignored when the glulam beam is subjected to stress. In the test, all the glulam beams are subjected to shear failure along the grain, thus the bearing performance of the glulam beam can be determined by its shear strength  $\tau$  [32]. Fig. 15 shows the distribution of shear stress in the cross section of a glulam beam, where  $Z$  is the distance from any point on the cross section to the neutral axis (mm). The shear stress on the cross section of the glulam beam is parabolically distributed along the thickness direction. For points at the upper and lower edges of the section, the shear stresses are zero. With the decrease in the distance from the neutral axis, the shear stress increases gradually and reaches a maximum at the neutral axis.

Neglecting the influence of the movement of neutral axis on the shear performance of glulam beam, the shearing strength ( $\tau$ ) of the web of glulam beam can be obtained by using Eq. (3) [33] as follows:

$$\tau = (F_z \times S_z)/(I_z \times d_1) \quad (3)$$

where  $F_z$  is the shear stress on the cross-section (kN),  $F_z = P_{\max}/2$ ,  $S_z$  is the static moment of the section ( $\text{mm}^3$ ),  $I_z$  is the inertial moment of the overall section to neutral axis ( $\text{mm}^4$ ), and  $d_1$  is the thickness of the web of glulam I-beam.

The shear stress mutual equal theory indicates that the vertical shear stress  $\tau$  of the micro unit is equal to the horizontal (parallel to the grain) shear stress  $\tau'$ . The maximum parallel-to-grain shear stress  $\tau_{\max}$  of the glulam beam section occurs at the neutral axis. When the maximum shear stress  $\tau'_{\max}$  of the neutral axis reaches the ultimate strength, the beam undergoes shear failure.

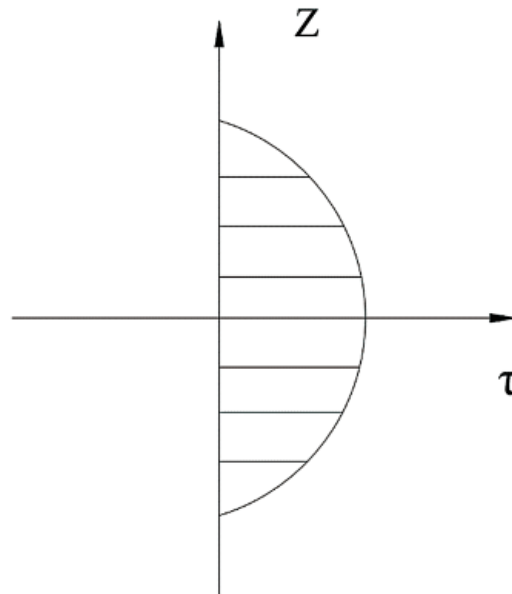


**Figure 15:** Distribution of shear stress

Soltis et al. [34] proposed the correlation for calculating the shear strength of glulam rectangular beam (see Eq. (4)).

$$\tau_b = 1.3 \times C_f \times \tau_m / A_s^{1/5} \quad (4)$$

where  $\tau_b$  is the shear strength of glulam beam (MPa),  $C_f$  is the stress concentration factor to adjust the damage strength of timber, which is taken as 2 according to the ASTM standard,  $\tau_m$  is the parallel-to-grain shear strength of the wood (MPa), and according to the material test mentioned above, the parallel-to-grain shear strength of larch wood is set to be 8.97 MPa. Similarly, the effective shear area (area of beam subjected to shear forces), can be calculated according to the correlation:

$$A_s = 5 \times B \times (t_1 + t_2) / 6 \quad (5)$$

where  $B$  is the width of the section (mm),  $t_1$  is the height of upper flange (mm), and  $t_2$  is the height of lower flange (mm). According to the ultimate load  $P_{\max}$  of the test specimen, the maximum parallel-to-grain shear stress  $\tau'_{\max}$  of the neutral axis could be obtained by using Eq. (3). This indicates that the experimental value of the ultimate bending shear stress is used, while the shearing strength  $\tau_b$  (theoretical value) of the beam is calculated according to the Soltis et al. [34] correlation (Eq. (4)). Based upon the calculations, the average shear strength  $\tau$  of group B1 is 4.41 MPa, while the value of  $\tau_b$  is 4.19 MPa. The experimental value of ultimate shear stress of the glulam beam is slightly larger than the theoretical value, indicating that the structural design has certain redundancy. The calculated results are in good agreement with the experimental values, and the relative error is within 10%, which indicates that the shear strength correlation proposed by Soltis et al. [34] is suitable not only for rectangular beams, but also for glulam I-beams.

#### 4 Conclusions

In this study, the flexural bearing capacity of 18 glulam I-beams was tested, and the load-deflection characteristics, load-strain relationship, and the parameters affecting the bearing capacity of the specimens were analyzed. According to the test results, the following conclusions are drawn.

1. When the depth-span ratio of the glulam beam is large (larger than 1/10) and the shear span ratio is small (less than 6), the typical failure mode at bending is the web shear failure parallel to grain. Before the failure, cracks and sounds appear at the beam web, which represent the sudden brittle failure.
2. The cross-sectional strain of the glulam beam is basically linearly proportional to the beam height, indicating that the plane section assumption is established. When the glulam beam enters the plastic stage, the neutral axis moves slowly toward the tension side, and the bending shear stress of the neutral axis becomes the largest. The crack of the shear failure occurs near the tension side of the initial neutral axis, which is consistent with the failure phenomenon.
3. Stiffener could improve the initial flexural stiffness of glulam beam, which experiences an increase of 28.21%. Larger the shear span ratio, smaller the initial flexural stiffness. The initial flexural stiffness improves by 10–23.5% with the increase in the thickness of the lower flange.
4. The effects of stiffener and shear-span ratio on shear strength are relatively significant. After the stiffeners are set at the support and the loading point in pairs, the shear strength of the glulam beam increases by 15.05% averagely. With the increase in the shear-span ratio, the shearing strength of the glulam I-beam gradually reduces. The equation of the shearing strength with the shear span ratio is obtained, which is shown by high fitting precision. The effect of flange thickness on the shear strength is relatively slight because of smaller span-depth ratio in the design of the test beams; moreover, all specimens are shear damaged and the strengths of the upper and lower flanges are not fully utilized. Therefore, it is recommended to increase the span-depth ratio in subsequent tests to investigate the effect of flange thickness on bearing performance under the flexural moment.
5. The shear strength correlation, as proposed by Soltis et al. [34], is suitable not only for rectangular beams, but also for glulam I-beams.

**Acknowledgement:** This research is supported by the Natural Science Foundation of Jiang-su Province (Grant No. BK20181402), the National Natural Science Foundation of China (Grant No. 51878354), a Project Funded by the National First-class Disciplines (PNFD), a Project Funded by the Priority Academic Program Development of Jiangsu Higher Education Institutions (PAPD), and a Project Funded by the Co-Innovation Center of Efficient Processing and Utilization of Forest Resources, Nanjing Forestry University (Nanjing, 210037, China). Any research results expressed in this paper are those of the writer(s) and do not necessarily reflect the views of the foundations. The authors greatly acknowledge Xiaojun Yang, Mingbin Liu, Xin Wang, Tongyu Hou, and others from the Nanjing Forestry University for helping with the tests.

**Conflicts of Interest:** The authors declare that they have no conflicts of interest to report regarding the present study.

## References

1. Sun, Y. F., Yang, X. J. (2011). On the development prospect of Chinese wood structural architecture. *Building Materials Decoration*, 6, 22–26.
2. He, M. J., Lam, F., Yang, J., Zhang, S. D. (2008). *Wood structural design*. Beijing: China Construction Industry Press.
3. Yuan, Z. F., Sun, Y. F. (2015). Thermal insulation materials for wood structures. *Decoration of Building Materials*, 6, 23–25.
4. Bigot, D., Ott, C., Guichard, S., Damour, B. M. (2019). Feasibility of using wood chips to regulate relative humidity inside a building: a numerical study. *Journal of Renewable Materials*, 7(6), 505–516. DOI 10.32604/jrm.2019.04019.
5. Li, H. T., Qiu, Z. Y., Wu, G., Corbi, O., Wang, L. B. et al. (2019). Slenderness ratio effect on eccentric compression performance of parallel strand bamboo lumber columns. *Journal of Structural Engineering ASCE*, 145(8), 04019077. DOI 10.1061/(ASCE)ST.1943-541X.0002372.

6. Li, H. T., Liu, R., Lorenzo, R., Wu, G., Wang, L. B. (2019). Eccentric compression properties of laminated bamboo columns with different slenderness ratios. *Proceedings of the Institution of Civil Engineers - Structures and Buildings*, 172(5), 315–326. DOI 10.1680/jstbu.18.00007.
7. Zhang, H. Z., Li, H. T., Corbi, I., Corbi, O., Wu, G. et al. (2018). AFRP influence on parallel bamboo strand lumber beams. *Sensors*, 18(9), 2854. DOI 10.3390/s18092854.
8. Li, X., Ashraf, M., Li, H. T., Zheng, X. Y., Wang, H. X. et al. (2019). An experimental investigation on parallel bamboo strand lumber specimens under quasi static and impact loading. *Construction and Building Materials*, 228, 116724. DOI 10.1016/j.conbuildmat.2019.116724.
9. Li, H. T., Qiu, Z. Y., Wu, G., Wei, D. D., Lorenzo, R. et al. (2019). Compression behaviors of parallel bamboo strand lumber under static loading. *Journal of Renewable Materials*, 7(7), 583–600. DOI 10.32604/jrm.2019.07592.
10. Tan, C., Li, H. T., Wei, D. D., Lorenzo, R., Yuan, C. G. (2019). Mechanical performance of parallel bamboo strand lumber columns under axial compression: experimental and numerical investigation. *Construction and Building Materials*, 231, 117168. DOI 10.1016/j.conbuildmat.2019.117168.
11. Wu, G. F., Zhong, Y., Gong, Y. C., Ren, H. Q. (2019). Application of modern wood product glulam in timber frame with tenon-mortise joints and its structural behavior. *Journal of Renewable Materials*, 7(5), 451–461. DOI 10.32604/jrm.2019.06229.
12. Moya, R., Valverde, L. F., Berrocal, A., Álvarez, D. M. (2017). Durability of thermally modified wood of *Gmelina arborea* and *Tectona grandis* tested under field and accelerated conditions. *Journal of Renewable Materials*, 3-4(3), 208–219. DOI 10.7569/JRM.2017.634111.
13. Ong, C. B. (2015). Glue-laminated timber (Glulam). *Wood Composites*, 123–140.
14. Stalnaker, J. J., Harris, E. C. (1997). Glued laminated members. *Structural Design in Wood*. 157–198.
15. Pulngern, T., Chucheeprakul, S., Padyenchean, C., Rosarpitak, V., Prapruit, W. et al. (2010). Effects of cross-section design and loading direction on the creep and fatigue properties of wood/PVC composite beams. *Journal of Vinyl and Additive Technology*, 16(1), 42–49. DOI 10.1002/vnl.20227.
16. Xiong, H. B., Kang, J. H., Lu, X. L. (2012). Experimental study on flexural behavior of wood composite beams. *Journal of Tongji University (Natural Science Edition)*, 40(04), 522–528.
17. Chen, G., Zhang, Q. S., Huang, D. S., Li, H. T. (2015). Experimental study on flexural properties of glued bamboo-wood I-beams. *Journal of Hunan University (Natural Science Edition)*, 42(05), 72–79.
18. Chen, G., Li, H. T., Zhou, T., Li, C. L., Song, Y. Q. et al. (2015). Experimental evaluation on mechanical performance of OSB webbed parallel strand bamboo i-joist with holes in the web. *Construction and Building Materials*, 101, 91–98. DOI 10.1016/j.conbuildmat.2015.10.041.
19. Hassanieh, A., Valipour, H. R., Bradford, M. A. (2016). Experimental and numerical study of steel-timber composite (STC) beams. *Journal of Constructional Steel Research*, 122, 367–378. DOI 10.1016/j.jcsr.2016.04.005.
20. Li, H. T., Wu, G., Zhang, Q. S., Deeks, A. J., Su, J. W. (2017). Ultimate bending capacity evaluation of laminated bamboo lumber beams. *Construction and Building Materials*, 160, 365–375. DOI 10.1016/j.conbuildmat.2017.11.058.
21. Shang, P. (2017). *Design and research of hollow beam-column system for plywood structural buildings (Ph.D. Thesis)*. Nanjing Forestry University. China.
22. Shang, P., Sun, Y. F., Zhou, D. G., Qin, K., Yang, X. L. (2018). Experimental study of the bending performance of hollow glulam beams. *Wood and Fiber Science*, 50(1), 3–19. DOI 10.22382/wfs-2018-002.
23. Wang, X. R., Zhou, A. P., Zhao, L. L., Chui, Y. H. (2019). Mechanical properties of wood columns with rectangular hollow cross section. *Construction and Building Materials*, 214, 133–142. DOI 10.1016/j.conbuildmat.2019.04.119.
24. Tang, Z., Shan, B., Li, W. G., Peng, Q., Xiao, Y. (2019). Structural behavior of glulam I-joists. *Construction and Building Materials*, 224, 292–305. DOI 10.1016/j.conbuildmat.2019.07.082.
25. ASTM D143. (2014). *Standard test methods for small clear specimens of timber*. West Conshohocken: ASTM International.

26. ANSI/AITC A190.1. (2012). *Structural for wood products-structural glued laminated timber*. ASTM International.
27. ASTM D198. (2015). *Standard test methods of static test of lumber in structural sizes*. ASTM International.
28. GB/T 28985. (2012). *Wood I-jioist for building structures*. China Building Industry Press.
29. GB/T 50005. (2017). *Code for design of timber structures*. China Building Industry Press.
30. Japan housing and wood technology center 1. (2005). *Design guide for the calculation of ultimate strength of wooden framed houses*. Tokyo: Co-operative Research Heng Society.
31. Que, Z. L., Yang, L., Zhao, D., Wang, Y. B., Wu, Y. (2014). Study on the performance of nail joints of wood shear wall under different overlaying conditions. *Architectural Structure*, 44(09), 93–96.
32. ASTM D905. (2003). *Standard test methods of static tests of lumber in structural size*. ASTM International.
33. Liu, H. W. (2008). *Concise mechanics of materials*. Beijing: Higher Education Press.
34. Soltis, L. A., Rammer, D. R. (1994). Shear strength of unchecked glued-laminated beams. *Forest Product Journal*, 44(1), 51–57.